Case Studies in Thermal Engineering 45 (2023) 102969

Contents lists available at ScienceDirect

Case Studies in Thermal Engineering

journal homepage: www.elsevier.com/locate/csite

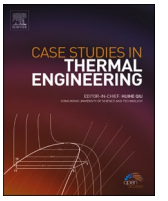

Investigating the thermal performance of air-cooling system integrated with TEC modules: Transient numerical simulation

Taif M. Mansoor [a], Saif W. Mohammed Ali [b,*], Hussam H. Jabbar [c]

[a] Sulaimani Polytechnic University, Sulaimani Technical Institute, Mechanic Department, Sulaymaniyah, Iraq
[b] University of Kufa, Faculty of Engineering, Department of Mechanical Engineering, Kufa, Najaf, Iraq
[c] Department of Cooling and Air Conditioning Engineering, Imam Ja'afar Al-Sadiq University, Baghdad, Iraq

HIGHLIGHTS

- Indirect non-evaporative cooling system integrated with TEC modules is studied numerically considering the transient effect.
- New derived dimensionless factor (HFR) is used to determine the thermal performance of the integrated system in addition to the wall heat flux and temperature difference under five different velocities.
- High temperature mode (HM), medium temperature mode (MM), and low temperature mode (LM) are the modes studied.
- HFR increases inversly with the inlet air velocity as time increases.
- Wall heat flux is higher for HM case at higher velocity while temperature difference is higher for HM case at lower velocity.

ARTICLE INFO

Keywords:
TEC modeling
Integrated-air conditioning system with TEC
Numerical study of TEC model
TEC units For space cooling
TEC as CPU cooler
Peltier and Seebeck effect

ABSTRACT

The current study represents a developed 3-D numerical transient model to a complete indirect non-evaporative cooling system integrated with an assisted TEC unit using OpenFOAM V.9 source code. The TEC model was developed using a hand-written code as a source added to the energy equation. The primary air temperature was a criterion to compare between three cases of environment's temperature: low mode (299 K), medium mode (309 K), and high mode (319 K). A new dimensionless factor called by Heat Flux Ratio (HFR) is derived to evaluate the thermal performance. In addition, wall heat flux and temperature difference along the vertical air channel were the parameters used for comparison. The complete system was constructed and validated according to number of experimental and theoretical studies from literature. Furthermore, all cases were tested under five different air inlet velocities: 0.75 m/s, 1 m/s, 1.25 m/s, 1.5 m/s, and 1.75 m/s. Results show that HFR values increase as time increases. In addition, it was found that HFR increases with the reduction in the velocity. Moreover, it was found that higher temperature difference can be reached at the lowest velocity (0.75 m/s) while the minimum difference would be at the highest velocity (1.75 m/s) with the error between modes doesn't pass (2.5%). On the other hand, the highest wall heat flux approached at the highest velocity (1.75 m/s) and vice versa where the error doesn't exceed (2.85%) between the modes. Finally, the validation shows good and acceptable agreement in COP values of the system with both experimental and theoretical works form literature where the error is ranged between (20.3% and 3.64%).

* Corresponding author.
E-mail address: saifw.alturaihi@uokufa.edu.iq (S.W. Mohammed Ali).

https://doi.org/10.1016/j.csite.2023.102969
Received 17 January 2023; Received in revised form 15 March 2023; Accepted 30 March 2023
Available online 15 April 2023

1. Introduction

In the light of global warming and the increase in demand of air-conditioning for buildings and facilities, the endeavors and effort to decrease the negative effect of air-conditioning and refrigeration compression cycle are still in early stage and not adequate to be replaced because of many obstacles and milestones. Additionally, the massive increase in demand of air conditioning (A/C) systems for building leads to increase in demand in the consumed power. For instance, the International Energy Agency (IEA) reported that 10% of global power consumption was utilized to operate 1.6 billion air conditioning units worldwide in 2016 [1]. Thus, intensifying the scientific research to develop a new air conditioning systems with less power consumption and less impact on global warming becomes a point of interest for all institutions involved to this field. The latest research to develop new air-conditioning and refrigeration systems is still underway and in progress.

The recent development of hybrid air cooling systems integrated with TED (Thermoelectric Devices) is one of the promising methods for air cooling with reducing the abovementioned negative impact of air-conditioning and refrigeration compression cycle. Thermoelectric Devices (TED's) are semiconductors that consist of two types of legs; P-type and N-type which are connected in electrical serial. Due to the Peltier effect (reverse of Sebeek effect), the arrangement will produce cooling in one side and heating in the other side. In order to get the benefit of this effect, each side is connected thermally in parallel. Recently, the system of TEDs' are used variously in different applications such as using TEC cooler to remove the heat form the microelectronic photo-detector (MPD) through looping of heat pipe (LHP) to maintain its temperature below 213 K [2]. Cooling and heating applications are the most widely applications where the TEDs are used [3–8]. The well-known indirect evaporative and non-evaporative cooling systems are the ones mostly integrated with TEDs as an air assisted cooler. TEDs unit cannot be used alone for large-scale air-conditioning systems as the efficiency of conversion of TEDs devices is very low [9]. Therefore, to make TEDs more efficient, they should be integrated with an assisted cooling system in such a way that the convenient conditions target for building can be reached. Thus, the current study focuses on investigating the performance of indirect non-evaporative cooling system integrated with TEC (Thermoelectric Cooler) coolers.

Cai Y. et al. [10]. developed a comprehensive numerical model to investigate the active cooling performance of phase change materials-base thermoelectric devices as PCM dynamic runs simultaneously with the TE conversion physics. The study used different parameters of PCM and TEDs to evaluate cooling performance in term of energy and exergy efficiencies. The study found that integrating PCM with TED's will enhance the cooling performance in different applications. Krishna et al. [11] performed an experimental study using PCM (Phase Change Material) as a cooling medium at the hot side of the thermoelectric device. Different parameters were studied and compared in this study like input voltage, velocity of air at hot side, PCM fill volume and configurations of heat sink (square pocket, rectangle pocket and circular pocket).The results showed that the heat sink with PCM reduced the temperature of the hot side of the thermoelectric cooler and the square pocket heat sink fully filled with PCM is better than other configurations which reduced the temperature of hot and cold sides of thermoelectric cooler from 68.3 $^{\circ}C$ and 34 $^{\circ}C$ respectively to 58.7 $^{\circ}C$ and 27 $^{\circ}C$ as compared to the heat sink without PCM at similar operating conditions.

Yang et al. [12] proposed a multi-TEC cooling modules by comping the TEC heat balance equations and thermal resistance matrix model and conducted an optimization process of power supply mode. They also used finite element simulation to verify and compare with the theoretical calculation. Their result showed that the theorical and simulation results are very close, and the optimal power supply mode depend on the multi-TEC configuration. The different substrate power consumptions will change the optimal current.

Ji R. et al. [13] Used multiple TECs to sterilize air ventilation form viruses. The work was done numerically using both sides of the TECs where the hot side is used to increase air temperature up to 65 °C while the cold side of the TECs was used to cool down the temperature of air to the conventional room temperature. Two types of surfaces were used to investigate the thermal performance of the system: smooth surface and finned surface. Nusselt number and friction factor were the parameters used for comparison. It was found that the studied system is sufficient to inactivate some viruses which are sensitive to temperature values up to 65 °C. In addition, it was found that the finned surface enhances the thermal performance of the system significantly.

An invented hybrid system proposed by many researchers in order to overcome the higher consumption power when dealing with higher cooling load. The hybrid cooling of air conditioning systems consists of direct and indirect evaporative cooling system assisted by TEC's. Those hybrid systems come in different configurations. Zhou Y. et al., 2021 [14] conducted an experimental and numerical simulation of indirect/thermoelectric assisted direct evaporative cooling system. The aim of the study was to investigate the influence of various operation parameters (i.e., inlet of the ambient temperature, relative humidity, velocity of inlet air, number of TEC modules … etc.). Their results showed that the experimental and simulation were agreed within +-10% error. These results allow them to theoretically optimize some of the operation parameters such as the current and number of TEC module, inlet velocity and mass flow rate in order to achieve high system performance.

The suggestion to overcome the high-power consumption of TEC's modules used to bring up the air to the comfortable room conditions was proposed by Zhou Y. et al. [15]. The same system configuration used by Zhou Y. et al. [14] was used in this experiment excluding the evaporative cooler and replace it with a spray water that is operating on demand order to decrease the temperature and increase the moisture content of the outlet air. another study by Zhou Y.et al. [16] introduced a mathematical model for their system to investigate the influence of the main operating geometrical parameters on the system. Their result shows that the system is able to keep relatively high COP depending on selected parameters.

Rohan B. et al. [17] Conducted a computational study for using phase change material in heat sink of the hot side of TEC module, their results showed that using different PCM types with different heat transfer coefficients and different heat sink geometries can reduce the temperature of the hot side significantly and contribute to justifying the thermal management of TECs.

Erdem C. et al. [18] conducted an experimental study on a novel water with nanofluid to air heat exchanger placed on the hot side of TEC. They used different nonfluid materials and the results showed that using Al2O3-water increases the performance of TEC in all

studied cases, because of its remarkable high thermal conductivity in compare with the other materials used in the study. Hani S. [19] studied the effect of output temperature and pressure drop of the hot side heat sink of TEC modules placed to cool lithium-ion battery cell. The study investigated the effect of using different geometrical shapes of fins placed in a channel saturated with alumina nanofluids. It was found that the output temperature and pressure drop depend on the fins' shape and the Reynolds number of the nanofluids

Pourkiaei et al. [20] in their review paper found that by increasing the figure of merit of TEC and developing the system setups, the TEC system can be used for residential air conditioning purposes. The improvement in TEC performance could be reached by establishing heat transfer model for the heat sink and its heat exchanger. Yang C. et al. [21] proposed an active thermoelectric ventilated system to cool a room space. They found in their optimization by comparison with traditional TEC; that for traditional TEC, the increase of TEC number will decrease the performance of the system. But by checking the entropy generation for the proposed system, the counter flow is better in cooling performance than the parallel flow between the cold and hot sides when the number of TEC be increasing.

Manikandan et al. [22] studied TEC for space cooling application but they used modified pulse operation mode, which means that a pulsed current input and pulsed heat transfer coefficient would be used for the hot side while a constant heat flux on the cold side. In their model, they used different pulse shapes and widths, and the results showed for typical operation conditions that the cooling power and COP increased by 23.3% and 2.12% higher than the normal operation conditions and the square shape pulse can provide higher cooling power and COP compared to other pulse shapes.

Buchalik and Nowak [23] Performed an experimental and theoretical analysis to investigate the feasibility of an air conditioning system integrated with TECs module both technically and economically. In term of technical investigation, COP and cooling capacity were the main parameters used in the study. On the other hand, new economic parameter called by "ETCC", or economic total cooling capacity was optimized to investigate the viability of the system. Results show that the optimized ETCC reaches about 58 W/$ in case of part load utilized power while ETCC increases to 0.64 W/$ if the cooling power load increases by 30%.

Srivastava et al. [24] investigated numerically a solar assisted TECs module which was integrated at a roof of a vehicle cabin. The system was studied under different inlet conditions and different solar tilt angles for cooling-heating purposes in different seasons. It was found that the new proposed system can reduce the cabin temperature by (17 $^{\circ}C$) in summer while the increase in temperature was about (15 $^{\circ}C$) in winter season at the optimum inlet conditions and optimum tilt angle.

Kim et al. [25] performed an experimental test to investigate an air-cooling integrated system with TECs module constructed with an automobile ceil to condition the rear seat passenger. The power supplied to the cooling integrated system was supported by using heat recovery system designed by integrating TEGs (thermoelectric generators) with the automobile exhaust system. Results show that the new integrated system can condition the rear space by an average of one passenger by reducing the temperature from 45 $^{\circ}C$ to 26 $^{\circ}C$.

Further studies were conducting to enhance the performance of thermoelectric generators (TEG) by looping of heat pipe systems (LHP). Experimental study was proposed by Suchen W. et al. [26] which compares the performance of TEG in case of integrating metal plate with the performance in case of using flat plate of heat piping network instead of metal plate. Three main factors were considered as criteria for comparison: heating power, inclination angle, and heating source size. It was concluded that the flat plate of the heat piping system increases the performance of the TEG significantly. Samson S. et al. [27] studied the effect of using flat plat heat pipe on

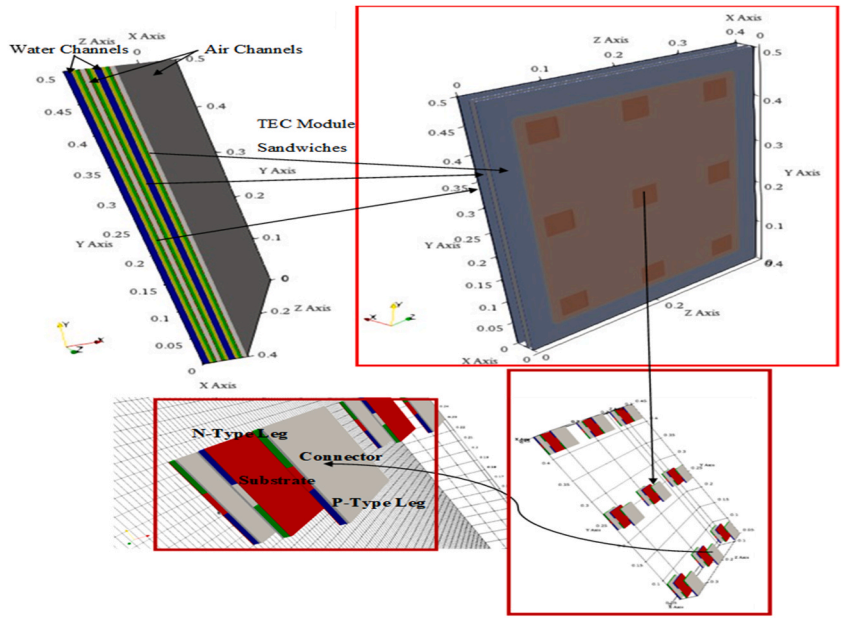

Fig. 1. Schematic diagram for the geometrical and physical domain of the studied system.

the performance of a hybrid photovoltaic-TEG system numerically. The study compared between two cases; with integrated flat plate heat pipe and without flat plate heat pipe. It was found that adding the flat plat heat pipe to the PV-TEG system enhances the efficiency of both the PV cell and the TEG module.

3-D numerical model of tabular arranging-TECs module was proposed for the first time by Xiao Tian et al. [28] around a tube bundle. The study was compared with flat-leg TECs modules to investigate its validity and favorability for HVAC systems. The hot side of the tabular TECs module was exposed to water flow while the cold side was exposed to air flow for cooling purposes. It was found that the performance of tabular TECs modules is much better than the flat-legs TECs module. In addition, it was found that the proposed system is suitable to be placed in HVAC systems.

Investigating the numerical transient effect on a complete three-dimensional (3-D) model of indirect non-evaporative cooling system integrated with TECs modules has not been studied yet in literature. Therefore, the main objective work of the current study is developing new numerical (3-D) model for a complete indirect non-evaporative cooling system integrated with TECs modules. OpenFOAM V.9 source code was used to investigate the transient effect on the thermal performance of the integrated system. Three different primary air inlet temperature cases were studied; low mode (LM) case where the inlet temperature approaching (299 K) representing the low temperature environment regions, medium mode (MM) case in which the primary inlet air temperature be around (309 K) when the environment temperature is moderate, and high mode (HM) case where the primary air inlet temperature be close to regions suffer the dry weather approaching (319 K). Furthermore, new dimensionless factor called by Heat Flux Ratio (HFR) was derived to determine the thermal performance of the whole integrated system.In addition, all cases (HM, LM, and MM) were studied and investigated under five different air inlet velocities: 0.75 m/s, 1 m/s, 1.25 m/s, 1.5 m/s, and 1.75 m/s. Wall heat flux and temperature difference along the air channel are the main parameters used for the comparison in addition to the new (HFR) factor. The tested integrated system was configurated and validated according to some experimental and theoretical works from literature.

2. Physical system description

All details involved the physical and geometrical domain of the studied system are shown in Fig. 1 The domain includes two channels of air as a working medium and two channels of water as a cooling medium. The face area of the air channel inlet is equal to (400 mm × 5 mm) while the face area of the water channel inlet is (500 mm × 7 mm). Air and water are flowing in a cross arrangement where air flows from the bottom to the top in y-direction while water flows perpendicularly in z-direction. Three sandwiches of TEC (Thermoelectric Cooler) modules were interfered through the channels in such a way that the hot side of the TEC modules faces the water channel while the cold side is exposed to the air channel. Aluminum plates, of (1 mm) thickness, are placed between the air channels and cold side of the TEC sandwiches while the thickness of the plates is (4 mm) between the water channels and TEC sandwiches. The TEC devices were placed in the TEC sandwiches in a way that each sandwich has three rows of TECs, each row contains three TEC devices. The TEC module used in the current simulation is based on the module named by (CPL4-127-06L). Number of thermos-couple is N' = 127 while each leg has a length of (Lt = 1.5 mm) and cross-sectional area of (At = 1.4 × 1.4 mm^2) [16]. Glass wool is placed as an insulation material between the TECs to reduce the heat losses. The thermophysical and electrical properties of the TECs, insulation material, Aluminum plates, and the flowing fluids are shown in Table 1.

3. Mathematical modeling and assumptions

3.1. Governing equations

The governing equations used in the current work can be categorized according to the sub-regions of the physical domain as below:

1 Governing equations involve the fluid region (Water channel and Air channel). The governing equations solved in fluid sub-regions are described as below:

3.1.1. Momentum equations

This equation characterizes the velocity and pressure distribution along the fluid domain in three dimensions [13,33]:

- **Momentum equation in the x-direction.**

Table 1
Thermophysical and Electrical Properties of all Materials and Fluids used in the current study [16,29–32].

Material or Fluid Type	Density (kg/m^3)	Specific Heat (kJ/kg.k)	Thermal Conductivity (W/m. k)	Seebeck Coefficient (V/k)	Resistivity (Ω.m)
Air	1.2	1004	0.0242	–	–
Water	1000	4181	0.561		
Aluminum	2700	871	237	–	–
Glass Wool (Insulation)	23	1800	0.038	–	–
TEC Module					
N-Type Leg	–	–	1.6	-210×10^{-6}	1×10^{-5}
P-Type Leg	–	–	1.6	210×10^{-6}	1×10^{-5}
Copper (Connector Plates)	8930	386	385	–	–

$$\frac{\partial u}{\partial t}+u\frac{\partial u}{\partial x}+v\frac{\partial u}{\partial y}+w\frac{\partial u}{\partial z}=-\frac{1}{\rho}\frac{\partial p}{\partial x}+\upsilon\nabla^2 u \tag{1}$$

- **Momentum equation in the y-direction.**

$$\frac{\partial v}{\partial t}+u\frac{\partial v}{\partial x}+v\frac{\partial v}{\partial y}+w\frac{\partial v}{\partial z}=-\frac{1}{\rho}\frac{\partial p}{\partial y}+\upsilon\nabla^2 v \tag{2}$$

- **Momentum equation in the z-direction.**

$$\frac{\partial w}{\partial t}+u\frac{\partial w}{\partial x}+v\frac{\partial w}{\partial y}+w\frac{\partial w}{\partial z}=-\frac{1}{\rho}\frac{\partial p}{\partial z}+\upsilon\nabla^2 w \tag{3}$$

3.1.2. Continuity equation

Continuity equation describes the mass conservation equation through the flow section. As the flow is assumed to be incompressible where flow density is considered as a constant, the continuity equation can be written as [33]:

$$\frac{\partial u}{\partial x}+\frac{\partial v}{\partial y}+\frac{\partial w}{\partial z}=0 \tag{4}$$

3.1.3. Energy transport equation in fluid

One of the equations used in the fluid regions is energy transport equation. Energy transport equation in fluid medium varies from energy transport equation in solid medium where in the fluid medium, the temperature values are driven by the momentum flux of the fluid. However, energy transport equation in the fluid region can be written as below [33]:

$$\frac{\partial T}{\partial t}+u\frac{\partial T}{\partial x}+v\frac{\partial T}{\partial y}+w\frac{\partial T}{\partial z}=\frac{k}{\rho C_p}\nabla^2 T \tag{5}$$

2 The other group of governing equations solved in the current work are the equations that relate the solid regions. In fact, solid regions, that are implemented in the construction of the current geometrical domain, are divided into three regions; solid region between the TEC model and the air channel (Air Solid Region), solid region between the TEC model and water channel (Water Solid Region), and finally, the solid region which lays within the scope of TEC model (TEC region).

Regarding the Air Solid Region (ASR) and Water Solid Region (WSR), energy transport equation is the only governing equation that should be solved. This energy transport equation is written as:

$$\frac{\partial T}{\partial t}=\frac{k}{\rho C_p}\nabla^2 T \tag{6}$$

On the other hand, Eq. (6) can be used in the TEC region to model the TEC integrated system using a source to simulate the TEC model as below [34,35], and [28]:

$$\frac{\partial T}{\partial t}=\frac{k}{\rho C_p}\nabla^2 T+\widehat{S}_{TEC} \tag{7}$$

Where $\widehat{S}_{TEC}$ represents the heat source which is added to the energy transport equation as a result to the integrated TEC unit. This can be written as:

- **In the n-type legs of the TEC model:**

$$\widehat{S}_{TEC}=\nabla.\left(\alpha_n T\vec{J}\right)+\dot{q} \tag{8}$$

$$\dot{q}=\vec{J}.\vec{E} \tag{9}$$

$$\vec{J}=\sigma_n\left(\vec{E}+\alpha_n\nabla T\right) \tag{10}$$

According to the math laws:

$$\nabla.(\alpha_n T)=\alpha_n\nabla T+\nabla\alpha_n T \tag{11}$$

By substituting Eq. (10) and Eq. (11) in Eq. (8), the final reformed equation would be:

$$\widehat{S}_{TEC}=\sigma_n^{-1}\vec{J}^{\,2}-\nabla\alpha_n T\,\vec{J} \tag{12}$$

- **In the p-type legs of the TEC model:**

Equations form (8) to (12) can be applied in the same context on the p-type legs except that (p) subscript would be used instead of using (n) subscript referring to that in the p-type legs, the electrical resistivity (σ) and the Seebeck coefficient (α) of the p-type material are the factors that should be used.

Thus, source term of the energy equation in p-type legs can be described as below.

$$\widehat{S}_{TEC} = \nabla.\left(\alpha_p T\vec{J}\right) + \dot{q} \tag{13}$$

$$\dot{q} = \vec{J}.\vec{E} \tag{14}$$

$$\vec{J} = \sigma_p\left(\vec{E} + \alpha_p \nabla T\right) \tag{15}$$

$$\nabla.\left(\alpha_p T\right) = \alpha_p \nabla T + \nabla \alpha_p T \tag{16}$$

$$\widehat{S}_{TEC} = \sigma_p^{-1}\,\vec{J}^{2} - \nabla \alpha_p T\,\vec{J} \tag{17}$$

- **In the substrate and connector parts of the TEC model:** the source term would be represented by the first term of Eq. (17) only as being shown below:

$\widehat{S}_{TEC} = \sigma_i^{-1}\,\vec{J}^{2}$ where (i) represents the electrical resistivity of the substrate part or connector part of the TEC model, accordingly. $\alpha, \sigma, and\ \vec{J}$ represent the Seebeck coefficient, electrical resistivity, and current density, respectively, while the voltage potential:

$$\vec{E} = -\nabla\varphi \tag{18}$$

Where (φ) is the voltage or the electric field potential.

- **Boundary Conditions.**

The physical domain of the current work is somehow complex due to using more than one fluid medium (air at the cold side, and water at the hot side) in addition to using different solid regions characteristics; solid plate between the fluid mediums and the TEC model sandwiches, and the solid plate within the scope of the TEC models, in which, equations from (7) to (18) would be applied in the mathematical model. However, the boundary conditions used in the current work are applied according to Fu R. et al. [36] and Sun D. et al. [37] as being shown below.

- At the inlet of air and water channels, the following boundary conditions would be applied.

a. Velocity and energy boundary conditions in fluid regions.

At the inlet of water channel along z-direction:

w_{in} = constant

While at the other directions:

$u = 0$, and $v = 0$.

On the other hand, the air inlet velocity along y-direction is:

v_{in} = constant

while at the other directions:

$w = 0$, and $u = 0$.

Similarly, the temperature values at the channels' inlet are:

$Tin\,|_{\text{air channel inlet.}}$ = constant.

$Tin\,|_{\text{water channel inlet}}$ = constant.

At the outlet of the fluid channels, zero gradient boundary conditions are applied for all physical characteristics as below:

$$\frac{\partial u}{\partial n}\Big|_{channel\ outlet} = \frac{\partial v}{\partial n}\Big|_{channel\ outlet} = \frac{\partial w}{\partial n}\Big|_{channel\ outlet} = 0$$

$$\frac{\partial T}{\partial z}|_{water\ channel\ outlet} = \frac{\partial T}{\partial y}|_{air\ channel\ outlet} = 0$$

Where (n) represents the direction in which velocity gradient would be taken.

b. Energy boundary conditions in solid regions.

Energy transport equation is the only equation applied in the solid region. In the TEC model, combining the equations from (7) to (18) gives a source which is added to the energy transport equations in the TEC region. Thus, the boundary conditions in the solid regions and TEC model can be written as below:

At the cold side of the TEC model:

$T|_{tec\text{-}cold\ side} = T_c$ (the initial cold temperature)

While at the hot side of the TEC model:

$T|_{tec\text{-}hot\ side} = T_h$ (the initial hot temperature)

At the interface between the TEC model and solid regions:

$$T|_{\text{TEC-Interface}} = T|_{\text{Solid-Interface}}$$

$$k_{TEC}\frac{\partial T}{\partial x}|_{TEC-interface} = k_{solid}\frac{\partial T}{\partial x}|_{TEC-interface}$$

Similarly, at the interface between the solid region and the fluid:

$$T|_{\text{Fluid-Interface}} = T|_{\text{Solid-Interface}}$$

$$k_{Solid}\frac{\partial T}{\partial x}|_{Fluid-interface} = k_{solid}\frac{\partial T}{\partial x}|_{Solid-interface}.$$

All other boundaries submit to the zero gradient and no slip conditions. This can be written as below:

$$\frac{\partial T}{\partial x} = \frac{\partial T}{\partial y} = \frac{\partial T}{\partial z} = 0$$

$$and, u = v = w = 0$$

The heat absorbed from air channel (Qc) can be calculated as below [38]:

$$Q_c = \alpha_m\, JT_c + \left(\frac{1}{2}\right) J^2\, \sigma_m - K_m\,(T_h - T_c) \tag{19}$$

On the other hand, the heat diffused in the cooling medium at the hot side of the studied cooling system can be calculated as below [38]:

$$Q_h = \alpha_m\, J\, T_h + \left(\frac{1}{2}\right) J^2\, \sigma_m - K_m\,(T_h - T_c) \tag{20}$$

The power employed to drive the heat in the TEC model represents the difference between both the (Q_h *and* Q_c) as:

$$P_{electric} = J.E = Q_h - Q_c \tag{21}$$

$\alpha_m, \sigma_m,$ *and* K_m were calculated by X. Gaoju et al. [38] as below:

$$\alpha_m = \frac{E_{max}}{T_{ho}}, \sigma_m = \frac{(T_{ho} - \Delta T_{max})}{J_{max}} \times \alpha_m, K_m = \frac{(T_{ho} - \Delta T_{max})}{2 \times \Delta T_{max}} \times \alpha_m \times J_{max}$$

The coefficient of performance (COP) of the cooling system can be calculated as below:

$$\text{COP} = \frac{Q_c}{P_{electric}} \tag{22}$$

$E_{max}, J_{max}, T_{ho},$ *and* ΔT_{max} are constants provided by the manufacturer of each TEC model which are shown in Table 2.

Table 2
The Properties of the TEC model used in the current study [16].

Factor	J_{max}	E_{max}	$J_{Applied}$	T_{ho}	ΔT_{max}	Q_{max}
Dimension	*Amber*	*Volt*	*Amber*	*K*	*K*	*Watt*
Value	6.0	15.4	1.0	299	67	51.4

4. Heat flux ratio (HFR)

One of the novel contributions of the current work is deriving new dimensionless factor called by Heat Flux Ratio (HFR). Utilizing dimensionless factors in scientific studies is one of the important approaches to reduce the dependent variables giving a complete picture about any change in the studied system by using a smaller number of parameters. However, (HFR) factor is calculated from the ratio between the overall heat flux removed from the fluid to the heat flux toward the TECs model. This can be determined as below:

$$\ddot{q}_x = f\left(\Delta T, L, K_{air}, \frac{\partial T}{\partial x}\right) \tag{23}$$

Where $\ddot{q}_x$ represents the heat flux toward the TEC module, ΔT is the temperature difference of working fluid between the inlet and the outlet, , L is the channel length, K_{air} is the air thermal conductivity, and $\frac{\partial T}{\partial x}$ is the temperature gradient in x-direction toward the TEC module.

Using Buckingham theorem to derive the dimensionless factors shows that:

N = number of parameters $(\ddot{q}_x, \Delta T, L, K_{air}, and\ \frac{\partial T}{\partial x}) = 5$

M = number of dimensions $(Mass\ (M), Length(L), Temperature\ (T), and\ Time(t)) = 4$

Number of possible derived factors = N -M = 5-4 = 1 = $A = \pi_i$.

$$\mathrm{M}^0 . \mathrm{L}^0 . \mathrm{T}^0 . \mathrm{t}^0 = (\Delta T\ (T))^a . (L\ (L))^b . (\ddot{q}_x(M.t^{-}3))^c . \left(, \frac{\partial T}{\partial x}(T.L^{-}1)\right)^d . K_{air}\left(M.t^{-3}.\mathrm{L}.t^{-}1\right) \tag{24}$$

Solving the above equation gives:

c = −1, d = 0, b = −1, and a = 1

From all above, and by assuming that π_i = HFR, it can be concluded that:

$$\mathrm{HFR} = \frac{K_{air}\frac{\Delta T}{L}}{\ddot{q}_x} = \frac{K_{air}\frac{\Delta T}{L}}{K_{air}\ddot{}\ \frac{\partial T}{\partial x}} = \frac{K_{air} * \frac{\left(T_{fluid-in} - T_{fluid-out}\right)}{Channel\ length}}{K_{air}\ \frac{\partial T}{\partial x}} = \frac{Q_{removed-Fluid}}{Q_{c-TECs}} \tag{25}$$

Thus,

$$HFR = \frac{Q_{removed-Fluid}}{Q_{c-TECs}} \tag{26}$$

Equation (26) can be expanded in the other two directions. However, as the walls in the z-direction are insulated, heat transfer is neglected in the z-direction. In addition, as the heat is only removed by the TEC module in x-direction, $\ddot{q}_y$ in flow direction will not be considered.

4.1. Numerical modeling and schemes

In the current study, OpenFOAM source code (Open-Source Field Operation and Manipulation) [39] was used to generate the mesh of the physical domain and solve the related mathematical modeling. OpenFOAM is a finite volume method (FVM) based solver and developed under the GL (General License) agreement. Different governing equations were implemented in the current model to find a suitable solution for the current indirect cooling system model integrated with TEC (thermoelectric cooler) model as was detailed previously. However, the presented numerical model was solved under assumptions shown below:

1 The solver used is transient solver.
2 All thermophysical properties are constants where *Cp, ρ, K,* α_t, and μ have been taken as constants in the current model.
3 The flow is considered as an incompressible flow for both the cold side (where air is the fluid which should be cooled) and the hot side (where water is used as a cooling medium).
4 The flow was assumed to be laminar.
5 The thermoelectric properties of the TEC are constants. This assumption means that σ_e and α_e are taken as constants through the electrical model.
6 Seebeck effect and conductivity effect are neglected in the connector and load surfaces.

Euler transient scheme was used to discretize the local or substantial derivative terms of the governing equations. Regarding the numerical schemes utilized for the special derivative term, there are different schemes used in the presented model; gauss upwind scheme, which represents a second order scheme, used to discretize the momentum equation in the fluid regions while gauss linear scheme was used to discretize the energy equation in both the fluid and solid regions including the electric potential source. Different numerical solution methods were used to solve the equation sets generated by the numerical schemes mentioned above. GAMG (Generalized Geometric-Algebraic Multigrid) solver was used to solve the pressure and energy schemes while diagonal solver was used to solve the explicit schemes. On the other hand, PBiCGStab (Preconditioned bi-conjugate Gradient) solver was used to solve the velocity and enthalpy schemes in the fluid regions. There are three different algorithms used to link between the pressure and velocity schemes in OpenFOAM; PISO (Pressure-Implicit Split Operator), SIMPLE (Semi-Implicit Method for Pressure Linked Equation), and PIMPLE algorithm which compromises between the previous two ones. In the current study, PIMPLE algorithm was used for the

pressure velocity linkage. To keep the explicit solver as stable as possible, the maximum courant number was set as (1).

In addition, to avoid any divergence in the solution, adjustable time step option was activated. As a novel contribution for the current paper, TEC model was configurated separately using user defined and handwritten codes called "heatTransferTEC" model where this model was developed from built-in model in OpenFOAM source code called by "heat transfer" model, and then, compiled with OpenFOAM code using specific tool called by "wmake". All the required parameters mentioned in the TEC governing equations' section of this paper were uploaded to the "controlDict" and "fvModels" journal files as a part of the numerical case study files.

4.1.1. Mesh convergence study

In the presented study, there are different mesh sizes tested to investigate the sensitivity of the calculated variables to the change in mesh sizes. COP (Coefficient of Performance) parameter is the criteria to find out the final mesh size at which, COP parameter would not be affected, or the change is not significant. COP factor was chosen as it represents a dimensionless factor in which more than one variable is included. Thus, COP factor behavior gives indication toward the overall system performance. Fig. 2 shows the mesh domain of the whole system where the whole mesh was built using structured or uniform mesh utilizing hexahedral cell shape.

Table 3 demonstrates the change in the COP factor with different mesh sizes. Four different mesh sizes were investigated to mimic the value of COP at which the value would not be changed, or the change is not significant when the mesh size increases. The figure shows that COP value changes significantly as mesh size increases from course mesh (2894320 cells) to medium mesh (5432348 cells). As the mesh size increases further from fine mesh (6585673 cells) to very fine mesh (8437800 cells), COP value would be much less sensitive to the increase in mesh. Therefore, as the increase in COP factor is not significant when mesh size increases from fine mesh to very fine mesh, it can be said that the numerical domain starts to be mesh independent at the fine mesh size (6585673 cells). Thus, all numeric data and cases done in the presented study were investigated under fine mesh size case.

5. Validation

The model developed in the current study was validated with number of experimental and theoretical studies from literature that have similar applications under similar conditions and inlet potential current. As shown in Table 4, COP value gained from current study is very close from theoretical value obtained by Zhou Y. et al. [16] where the error reaches about 3.64% between both values while an experimental value gotten by Zhou Y. et al. [15] is higher than the value of the current study by about 20.3%. However, the error between the current value and other studies (Du CY., and Wen CD. [40] and Guo D. et al. [41]) is ranged from (8.5%–12.95%).

Overall, the agreement between the calculated COP value in the presented work and the experimental and theoretical values calculated by studies from literature is placed in an acceptable range as was shown above.

6. Results and discussion

The thermal behavior of indirect non-evaporative cooling system was investigated in the current paper using new approach of determination. HFR dimensionless factor was derived in the present study using the conventional dimensional analysis to be used for performance calculations as a novel contribution for the current study. In addition, wall heat flux and temperature difference were utilized as a criterion of comparison between different cases. In the current section, the data calculated would be demonstrated and

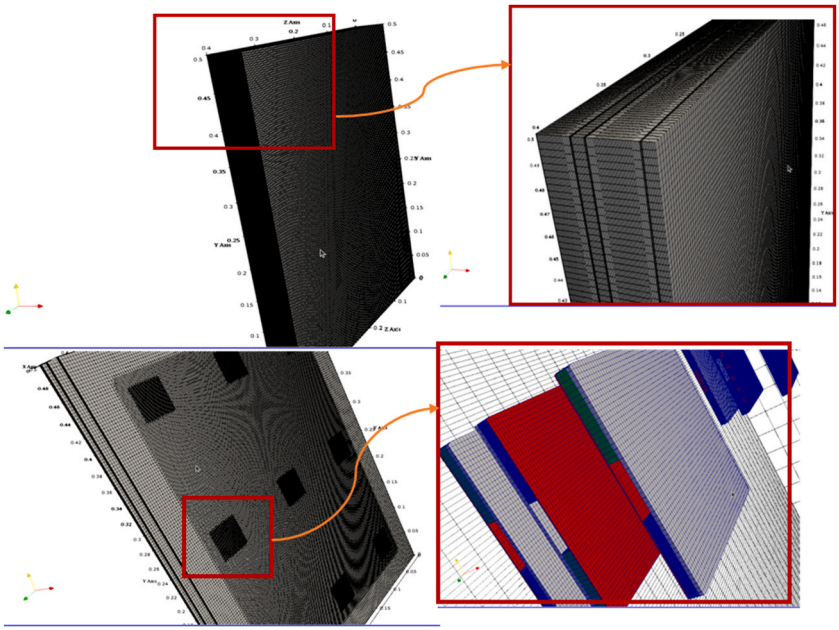

Fig. 2. Mesh domain for the whole system.

Table 3
COP parameter at different mesh sizes.

Mesh Size	COP value
2894320 cells	2.416484571
5432348 cells	2.454662649
6585673 cells	2.471561143
8437800 cells	2.476568104

Table 4
Comparison of COP value in the current study with studies from literature.

Research Work	COP value
Current Work study	2.47
Zhou Y. et al. [16] Theoretical 2018	2.38
Zhou Y. et al. [15] Experimental 2022	3.1
Du CY. [40] Experimental 2011	2.15
Guo D. [41] Theoretical 2020	2.7

discussed.

Fig. 3 (a, b, and c) shows the distribution of wall heat flux toward the TEC modules positions after (5 s), (10 s), and (15 s), respectively from the run starting point. The results were drawn under three air inlet velocities: a-) Vin = 0.75 m/s, b-) 1.25 m/s, and c-) 1.75 m/s result shows that wall heat flux decreases along the air channel from the inlet to the outlet at the same run time for all cases. This comes because of the reduction in the heat stored in the fluid as air flows through the channel form the bottom to the top causing the flux gradient along the channel. However, as velocity increases, the wall heat flux increases too at the same flow position. This likely happens as heat energy in the fluid region is driven by momentum flux unlike the heat energy in the solid region. Furthermore, it is found from these figures that wall heat flux increase along the channel as time goes forward, and this is why flux contour seems to be brighter as time changes from (5 s) to (10 s, and 15 s). An interesting finding is that the flux parabola at the horizontal line behaves in such a way that the flux starts lower and then increases exponentially and then decreases in symmetrical way. As time increases, the

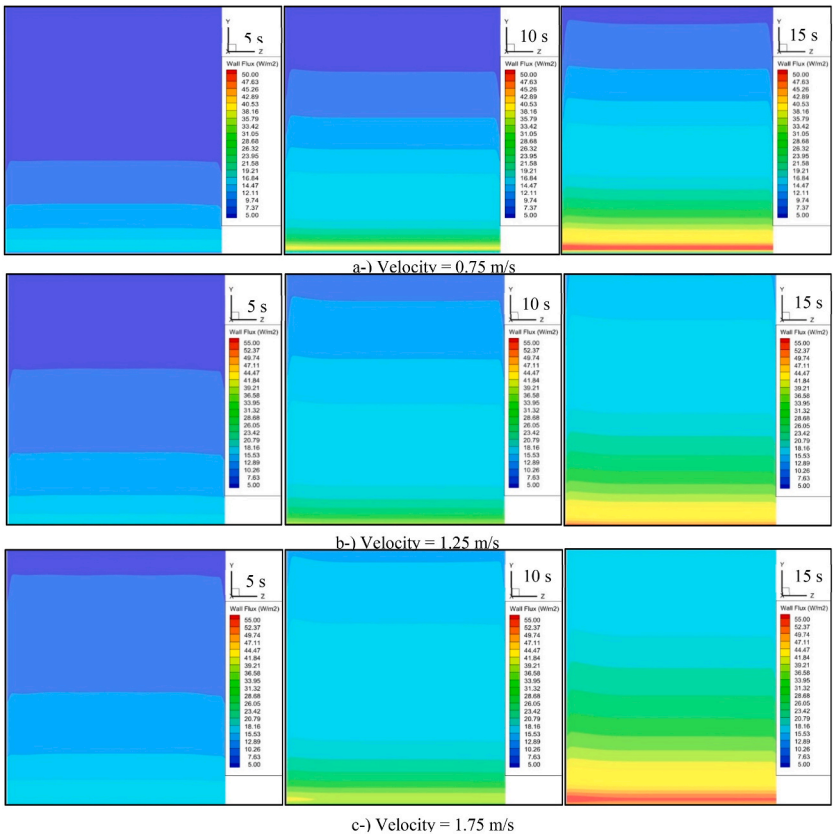

Fig. 3. Wall heat flux for HM case after (5 s), (10 s), and (15 s) from system run time under three different velocities; a-) 0.75 m/s, b-) 1.25 m/s, and c-) 1.75 m/s.

flux changes in such a way that the values increase and then decrease internally where the curve takes (M) shape to be decreasing finally. This comes as the TEC module works more efficiently as time increases where the TEC modules placed at the internal region away from the sandwich's boundaries. The wall flux values calculated in the present work are placed within the range of data reported by Yong-Kwon et al. [42] as a sufficient evident regarding the viability of the model solved in the current paper.

Fig. 4 shows the HFR distribution along the air channel after a-) 5 s, b-) 10 s, and c-) 15 s respectively, from the starting run time under four different velocities; 0.75 m/s, 1 m/s, 1.25 m/s, 1.5 m/s, and 1.75 m/s. It was found from the figure that HFR starts small reduction at the channel inlet, and then, it starts increasing for all cases. This comes likely as TEC devices starts to be placing at position equals to (0.05 m) from the channel inlet along the channel length. Therefore, there is no reduction in the temperature values as the TEC effect begins at small distances before the TEC region. Furthermore, it was found that as time increases, the HFR values increase too. For instance, it was found that the HFR value is about (0.03875) after (5 s) at velocity of (0.75 m/s) while the HFR value reaches about (0.053) and (0.056) after (10 s) and (15 s) respectively. An interesting finding is that the HFR values reduce as velocity increases after (5 s) while at (10 s), the HFR for velocity of (1.75 m/s) try to be dominant in compare with velocity of (1.5 m/s) and (1.75 m/s), and then, the behavior turns back to its initial state. This happens as at the medium time the TEC module has an efficient work while it approaches its maximum activity after (15 s) as has been shown previously that HFR after (5 s) is (0.053) where this value is very close to the HFR value after (15 s) which is equal to (0.056) while the initial HFR is (0.03875) after (5 s).

Fig. 5 (a and b) shows the temperature difference and wall heat flux along air channel at the middle line from channel inlet to channel outlet under five different velocities: 0.75 m/s, 1 m/s, 1.25 m/s, 1.5 m/s, and 1.75 m/s. The figure shows the values after (15 s) from run starting time. As the TECs module placed at (0.05 m) from channel inlet, temperature difference start increasing gradually from this point where at the channel inlet, the difference is very small because that the TEC effect is much lower in compare with its effect on flow after (0.05 m). Therefore, it can be seen obviously that the curve has a very steep gradient at the inlet while the temperature difference increases normally after that point till it reaches its maximum value at channel outlet. Another interesting

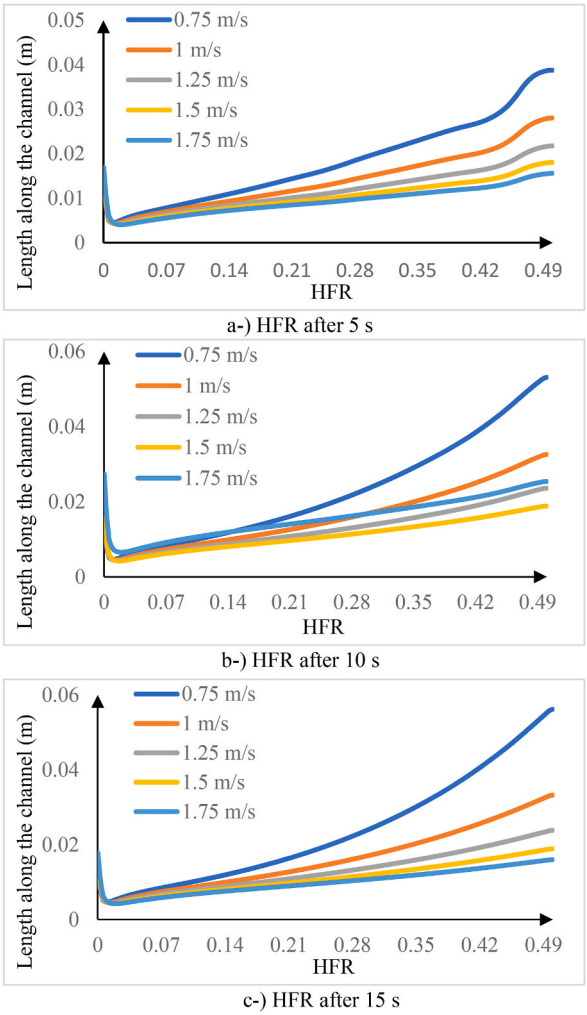

Fig. 4. HFR behavior along the air channel after a-) 5 s, b-) 10 s, and c-) 15 s from the starting run time for five different velocities; 0.75 m/s, 1 m/s, 1.25 m/s, 1.5 m/s, and 1.75 m/s.

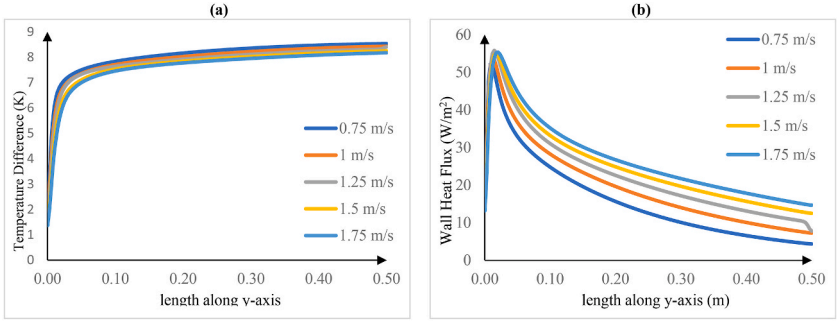

Fig. 5. Temperature Difference and wall heat flux distribution along air channel for all velocities after 15 s; a-) Temperature Difference, b-) Wall heat Flux.

finding is that as velocity increases, temperature difference decreases. This comes from the fact that as velocity be lower, more heat would be removed from the fluid and vice versa. However, it was found that the maximum value of temperature different is (8.62 K) at inlet velocity equals to (0.75 m/s) while the maximum temperature difference approaches (8.2 K) at inlet velocity equals to (1.75 m/s). Therefore, the maximum error between the minimum velocity and maximum velocity reaches about (4.87%) while the minimum error would be between V = 1.5 m/s and V = 1.75 m/s where this value reaches about (1.79%). As was shown in the figure, when air inlet velocity increases, the error in temperature difference between the consequent inlet velocities cases decreases because of that less velocity gives higher period for heat absorption while this period decreases as velocity increases velocity increases causing less error in case of higher velocities.

Fig. 5-b demonstrates wall heat flux distribution absorbed by TECs modules at the middle line of air channel for five different velocities after (15 s) from run starting time. It was found that wall heat flux starts its minimum value at air channel inlet, and then it approaches its maximum value at (0.05 m) from the channel inlet where the TECs modules placed at this distance from air channel inlet as was shown before. Then, wall heat flux starts decreasing exponentially along air channel. Such a behavior is expected because that heat latent in the fluid starts higher at the channel inlet leading to higher heat flux absorbed by the TECs module. As air flows vertically toward channel outlet, fluid latent heat decreases by the TECs modules causing less heat flux absorbed by the consequent TECs modules. In contract with temperature difference distribution mentioned in the previous section, wall heat flux changes directly with air inlet velocity although what have been mentioned before regarding velocity effect on period required for heat removing from fluid flow. This likely happens as that the increase in the velocity leads to increase in temperature gradient toward TECs sides as velocity contributes to the energy equation of fluid region causing higher flux as was shown in Eq. (5). The range of wall heat flux calculated in the current work is very close to values reported by Yong-Kwon et al. [42] assuring the validity of the present numerical work. The difference between wall heat flux values at different velocities is increasing as air flows vertically from channel inlet to channel outlet till it reaches its maximum value at channel outlet where the difference is equal to (70%) between case of V = 0.75 m/s and V = 1.75 m/s at channel outlet while that difference reaches about (7%) at channel inlet. Additional finding is that the difference between different consequent velocities cases is decreasing as velocity increases. In this context, the difference in wall heat flux between case of V = 1.75 m/s and case V = 1.5 m/s is (16.667%). On the other hand, the error reaches about (40%) between case of V = 0.75 m/s and case of V = 1 m/s where all these differences were calculated at channel outlet.

Fig. 6 (a, and b) shows temperature difference and wall heat flux behavior respectively. The figure shows the distribution along air channel form the inlet to the outlet under three different modes (LM, MM, and HM) when the air inlet velocity is equal to (V = 1.75 m/s). As was shown in Fig. 5-a, temperature difference starts its minimum values at the inlet where the effect of TECs modules is not significant while it starts increasing normally after distance of (0.05 m) where the TECs devices was placed. Therefore, the curves start steep lines while the gradient in the temperature difference behaves exponentially and normally after that distance. This behavior is applicable for all cases (LM, MM, and HM). For similar reasons mentioned above, curves of LM, MM, and HM are laid on each other at channel inlet. However, the minimum values of temperature difference for all modes are similar at the specified velocity. An interesting finding is that temperature gradient differs depending on the mode studied. For instance, it was found that higher temperature difference would be for case of HM and the lowest value would be for case of LM. Another finding is that the difference between modes increases along air channel till reaching its maximum value at channel outlet where the difference between each mode is about (2.5%). Fig. 6-b shows the wall heat flux for different modes (LM, MM, and HM) at (V = 1.75 m/s). In contradiction with the behavior of temperature difference, wall heat flux starts its maximum value at channel inlet after (0.05 m) for the similar reasons mentioned in Fig. 5-a while it decreases exponentially till it reaches its minimum value at channel outlet. It was found from the figure that HM case has higher heat flux values than other cases while LM has the smallest values where the maximum difference between modes reaches (4.5%).

7. Conclusion

A 3-D transient numerical model was developed in the current study to investigate the thermal performance of an indirect non-evaporative cooling system integrated with a TECs integrated units using OpenFOAM V.9 source code. The TECs model was developed in the current study using a hand-written code which was implemented and compiled with the OpenFOAM solver used in the current simulation. The main novelty of the current study is represented by deriving new dimensionless parameter called by heat flux

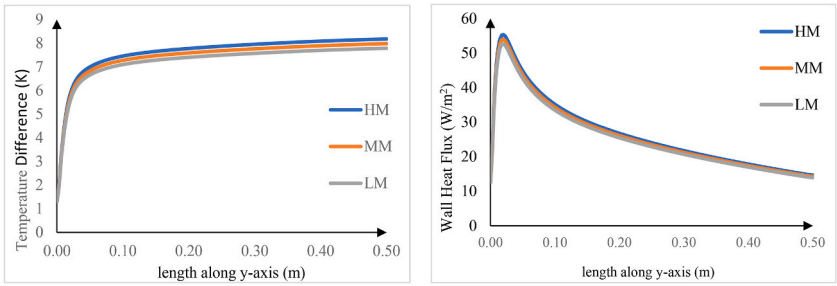

Fig. 6. Temperature Difference and wall heat flux distribution along air channel for all modes after 15 s and air inlet velocity = 1.75 m/s; a-) Temperature Difference, b-) Wall heat Flux.

ratio (HFR) to determine the performance of the system. The whole integrated system was investigated under three main scenarios; the case of (299 °*K*) as an inlet primary air temperature for low environment temperature regions or what is called by low mode (LM), the case of inlet primary air temperature equals to (309 °*K*) or the medium mode case (MM), and the high mode (HM) case in which the inlet primary air temperature approaching the (319 °*K*) threshold. All cases were tested under five different air inlet velocities: 0.75 m/s, 1 m/s, 1.25 m/s, 1.5 m/s, and 1.75 m/s. It was concluded from the results that HFR increases as time increases till it reaches its stable values after (15 s) in the current work. In addition, as time goes further, it was concluded that HFR for lowest velocities increases to be higher than the HFR values at the higher velocities. Regarded the effect of inlet air velocities, it was concluded that the increase in velocity affects negatively the temperature difference along the vertical air channel where it was found that temperature difference at velocity equals to (0.75 m/s) is higher than the temperature difference at velocity equals to (1.75 m/s) by about (4.87%) while the temperature difference at velocity (1.5 m/s) is higher than the temperature difference at (1.75 m/s) by about (1.79%). In opposite with temperature difference, the increase in the air inlet velocity leads to increase in wall heat flux. Furthermore, it was concluded that the difference in wall heat flux between different velocities cases is increasing along the air channel where wall heat flux at (1.75 m/s) is higher than the flux in case of (0.75 m/s) by about (7%) at channel inlet while the percentage increases to (70%) at channel outlet. Regarding the effect of different modes on temperature difference and wall heat flux, it was concluded that wall heat fluxes and temperature differences are higher at higher modes and vice versa. For example, temperature difference for HM case is higher than this value for the MM case by about (2.34%) at velocity equals to (0.75 m/s) while this percentage increases to (2.5 m/s) for case of (1.75 m/s). On the other hand, the difference reaches about (2.85%) and (4.5%) in wall heat flux for the cases of (0.75 m/s) and (1.75 m/s), respectively. The error in COP between the current study and previous studies is ranged from (20.3%–3.64%) where this range is agreeable and acceptable.

Author statement

Taif M. Mansoor: Writing, Review, Editing, and Investigation, Formal Analysis. **Saif W. Mohammed Ali:** Writing, Editing, Methodology, Data curation, Formal Analysis. **Hussam H. Jabbar:** Conceptualization, Writing, Editing, Review, Investigation, Resources.

Declaration of competing interest

The authors declare that they have no known competing financial interests or personal relationships that could have appeared to influence the work reported in this paper.

Data availability

Data will be made available on request.

Acknowledgement

This work was supported by the faculty of engineering at university of Kufa, Sulaimani polytechnic university, and Imam Ja'afer Al-Sadiq university. The authors are very thankful for their support.

Nomenclatures

u, v, w	Velocities in x, y, z directions respectively (m/s)
p	Pressure (pa)
T	Time (sec)
T	Temperature (°*K*)
k	Thermal Conductivity (W/m. °*K*)

C_p	Heat Capacity (J/kg. $^\circ K$)
$\widehat{S}_{TEC}$	Source of TEC model added to the energy equation
$\vec{J}$	Current Density (Amber)
$\vec{E}$	Electric Voltage (Voltage)
$\dot{q}$	Heat generated (W/m^3)
Q	Heat removed or generated by TEC (W)
$P_{electric}$	Electric Power (W)
x, y, z	Spatial distances in the cartesian coordinate system

Abbreviations

HFR	Heat Flux Ration
HM	High Mode
MM	Medium Mode
LM	Low Mode
COP	Coefficient of Performance
TEC	Thermoelectric Cooler
TED	Thermoelectric Device
IEA	International Energy Agency
PCM	Phase Change Material
ETCC	Economic Total Cooling Capacity
HVAC	Heating-Ventilating-Air Conditioning
TEG	Thermoelectric Generator
ASR	Air Solid Region
WSR	Water Solid Region

GREEK SYMBOLS

υ	Kinematic Viscosity (m^2/s)
$\boldsymbol{\rho}$	Density (kg/m^3)
∇	Gradient Operator
α	Seebeck Coefficient (Vol/ $^\circ K$)
σ	Electric Resistivity (Ω.m)
φ	Electric PotentialSubscripts
N	N-type leg of the TEC
p	P-Type leg of the TEC
c	Cold side of TEC
h	Hot side of TEC
ho	Initial hot temperature

References

[1] International Energy Agency Report, The Future of Cooling Opportunities for Energy-Efficient Air Cooling, 2018.

[2] Boris I. Basok, Yurii E. Nikolaenko, Roman S. Melnyk, Thermal management of electronic devices using heat pipes (Chapter 3), in: Yuwen Zhang (Ed.), Heat Pipes: Design, Application, and Technology, Nova Science Publisher, Inc., NY., USA, 2018, pp. 203–253.

[3] M. Zebarjadi, K. Esfarjani, M.S. Dresselhaus, Z.F. Ren, G. Chen, Perspectives on thermoelectrics: from fundamentals to device applications, Energy Environ. Sci. 5 (1) (2012) 5147–5162, https://doi.org/10.1039/c1ee02497c.

[4] X.F. Zheng, C.X. Liu, Y.Y. Yan, Q. Wang, A review of thermoelectrics research – recent developments and potentials for sustainable and renewable energy applications, Renew. Sustain. Energy Rev. 32 (2014) 486–503, https://doi.org/10.1016/j.rser.2013.12.053.

[5] N. Miljkovic, E.N. Wang, Modeling and optimization of hybrid solar thermoelectric systems with thermosyphons, Sol. Energy 85 (11) (2011) 2843–2855, https://doi.org/10.1016/j.solener.2011.08.021.

[6] H.S. Huang, Y.C. Weng, Y.W. Chang, S.L. Chen, M.T. Ke, Thermoelectric water-cooling device applied to electronic equipment, Int. Commun. Heat Mass Tran. 37 (2) (2010) 140–146, https://doi.org/10.1016/j.icheatmasstransfer.2009.08.012.

[7] Y.W. Chang, C.C. Chang, M.T. Ke, S.L. Chen, Thermoelectric air-cooling module for electronic devices, Appl. Therm. Eng. 29 (13) (2009) 2731–2737, https://doi.org/10.1016/j.applthermaleng.2009.01.004.

[8] Wan Q. shi, J jun Su, Y yi Huang, Y ping Wang, X. Liu, Numerical and experimental investigation on symmetrical cross Jet of localized air conditioning system with thermoelectric cooling devices in Commercial vehicles, Int. J. Refrig. 140 (2022) 29–38, https://doi.org/10.1016/j.ijrefrig.2022.05.004.

[9] S.M. Pourkiaei, M.H. Ahmadi, M. Sadeghzadeh, S. Moosavi, F. Pourfayaz, L. Chen, et al., Thermoelectric cooler and thermoelectric generator devices: a review of present and potential applications, modeling and materials, Energy 186 (2019), 115849, https://doi.org/10.1016/j.energy.2019.07.179.

[10] Y. Cai, B.H. Hong, W.X. Wu, W.W. Wang, F.Y. Zhao, Active cooling performance of a PCM-based thermoelectric device: dynamic characteristics and parametric investigations, Energy 254 (2022), 124356, https://doi.org/10.1016/j.energy.2022.124356.

[11] N. Vijay Krishna, S. Manikandan, C. Selvam, Enhanced performance of thermoelectric cooler with phase change materials: an experimental study, Appl. Therm. Eng. 212 (2022), 118612, https://doi.org/10.1016/j.applthermaleng.2022.118612.

[12] H. Yang, J. Zhang, G. Xia, H. Zhao, X. Song, Analysis of air-cooling module with multi-TEC, Int. Commun. Heat Mass Tran. 134 (2022), 106041, https://doi.org/10.1016/j.icheatmasstransfer.2022.106041.

[13] R. Ji, T. Pan, G. Peng, J. Ma, N. Yang, Q. Hao, An integrated thermoelectric heating-cooling system for air sterilization— a simulation study, Mater. Today Phys. 19 (2021), 100430, https://doi.org/10.1016/j.mtphys.2021.100430.
[14] Y. Zhou, Z. Yan, Q. Dai, Y. Yu, Experimental and numerical evaluation of a two-stage indirect/thermoelectric assisted direct evaporative cooling system, Energy Convers. Manag. 248 (2021), 114780, https://doi.org/10.1016/j.enconman.2021.114780.
[15] Y. Zhou, Z. Yan, Q. Dai, Y. Yu, Experimental study on the performance of a novel hybrid indirect evaporative cooling/thermoelectric cooling system, Build. Environ. 207 (2022), 108539, https://doi.org/10.1016/j.buildenv.2021.108539.
[16] Y. Zhou, T. Zhang, F. Wang, Y. Yu, Performance analysis of a novel thermoelectric assisted indirect evaporative cooling system, Energy 162 (2018) 299–308, https://doi.org/10.1016/j.energy.2018.08.013.
[17] R. Bhuiya, N. Shah, D. Arora, N.V. Krishna, S. Manikandan, C. Selvam, et al., Thermal management of phase change material integrated thermoelectric cooler with different heat sink geometries, J. Energy Storage 51 (2022), 104304, https://doi.org/10.1016/j.est.2022.104304.
[18] E. Cuce, T. Guclu, P.M. Cuce, Improving thermal performance of thermoelectric coolers (TECs) through a nanofluid driven water to air heat exchanger design: an experimental research, Energy Convers. Manag. 214 (2020), 112893, https://doi.org/10.1016/j.enconman.2020.112893.
[19] H. Sait, Cooling a plate lithium-ion battery using a thermoelectric system and evaluating the geometrical impact on the performance of heatsink connected to the system, J. Energy Storage 52 (2022), 104692, https://doi.org/10.1016/j.est.2022.104692.
[20] S.M. Pourkiaei, M.H. Ahmadi, M. Sadeghzadeh, S. Moosavi, F. Pourfayaz, L. Chen, et al., Thermoelectric cooler and thermoelectric generator devices: a review of present and potential applications, modeling and materials, Energy 186 (2019), 115849, https://doi.org/10.1016/j.energy.2019.07.179.
[21] Y. Cai, L. Wang, W.T. Ding, D. Liu, F.Y. Zhao, Thermal performance of an active thermoelectric ventilation system applied for built space cooling: network model and finite time thermodynamic optimization, Energy 170 (2019) 915–930, https://doi.org/10.1016/j.energy.2018.12.186.
[22] S. Manikandan, S.C. Kaushik, R. Yang, Modified pulse operation of thermoelectric coolers for building cooling applications, Energy Convers. Manag. 140 (2017) 145–156, https://doi.org/10.1016/j.enconman.2017.03.003.
[23] R. Buchalik, G. Nowak, Technical and economic analysis of a thermoelectric air conditioning system, Energy Build. 268 (2022), 112168, https://doi.org/10.1016/j.enbuild.2022.112168.
[24] R.S. Srivastava, A. Kumar, H. Thakur, R. Vaish, Solar assisted thermoelectric cooling/heating system for vehicle cabin during parking: a numerical study, Renew. Energy 181 (2022) 384–403, https://doi.org/10.1016/j.renene.2021.09.063.
[25] D hye Kim, S. Seo, S. Kim, S. Shin, K. Son, S jae Jeon, et al., Design and performance analyses of thermoelectric coolers and power generators for automobiles, Sustain. Energy Technol. Assessments 51 (2022), 101955, https://doi.org/10.1016/j.seta.2022.101955.
[26] W. Suchen, D. Yiwen, Z. Chengbin, X. Dehao, Improving the performance of a thermoelectric power system using a flat-plate heat pipe, Chin. J. Chem. Eng. 27 (2019) 44–53, https://doi.org/10.1016/j.cjche.2018.03.019.
[27] S. Samson, L. Guiqiang, Z. Xudong, G.A. Yousif, M. Xiaoli, Y. Min, Comparative Study of a concentrated photovoltaic-thermoelectric system with and without flat plate heat pipe, Energy Convers. Manag. 193 (2019) 1–14, https://doi.org/10.1016/j.enconman.2019.04.055.
[28] X.X. Tian, S. Asaadi, H. Moria, A. Kaood, S. Pourhedayat, K. Jermsittiparsert, Proposing tube-bundle arrangement of tubular thermoelectric module as a novel air cooler, Energy 208 (2020), 118428, https://doi.org/10.1016/j.energy.2020.118428.
[29] H. Ruan, H. Xie, J. Wang, J. Liao, L. Sun, M. Gao, et al., Numerical investigation and comparative analysis of nanofluid cooling enhancement for TEG and TEC systems, Case Stud. Therm. Eng. 27 (2021), 101331, https://doi.org/10.1016/j.csite.2021.101331.
[30] E. Söylemez, E. Alpman, A. Onat, S. Hartomacıoğlu, CFD analysis for predicting cooling time of a domestic refrigerator with thermoelectric cooling system, Int. J. Refrig. 123 (2021) 138–149, https://doi.org/10.1016/j.ijrefrig.2020.11.012.
[31] S. Madruga, Modeling of enhanced micro-energy harvesting of thermal ambient fluctuations with metallic foams embedded in Phase Change Materials, Renew. Energy 168 (2021) 424–437, https://doi.org/10.1016/j.renene.2020.12.041.
[32] S. Fan, A. Rezania, yuanwen Gao, Thermal-electric and stress analysis of thermoelectric coolers under continuous pulse input current, Appl. Therm. Eng. 214 (2022), 118910, https://doi.org/10.1016/j.applthermaleng.2022.118910.
[33] Frank W. White, Fluid Mechanics, fifth ed., McGraw-Hill Companies, Inc., New York, 2003.
[34] Wan Q. shi, J jun Su, Y yi Huang, Y ping Wang, X. Liu, Numerical and experimental investigation on symmetrical cross Jet of localized air conditioning system with thermoelectric cooling devices in Commercial vehicles, Int. J. Refrig. 140 (2022) 29–38, https://doi.org/10.1016/j.ijrefrig.2022.05.004.
[35] D. Luo, R. Wang, Y. Yan, W. Yu, W. Zhou, Transient numerical modelling of a thermoelectric generator system used for automotive exhaust waste heat recovery, Appl. Energy 297 (2021), 117151, https://doi.org/10.1016/j.apenergy.2021.117151.
[36] R.P. Fu, Z.G. Qu, W.Q. Tao, X.B. Zhu, J.R. Liu, Experimental and numerical study on performance of hybrid refrigeration system that combines vapor compression and thermoelectric systems, Appl. Therm. Eng. 194 (2021), 117107, https://doi.org/10.1016/j.applthermaleng.2021.117107.
[37] D. Sun, L. Shen, H. Chen, B. Jiang, D. Jie, H. Liu, et al., Modeling and analysis of the influence of Thomson effect on micro-thermoelectric coolers considering interfacial and size effects, Energy 196 (2020), 117116, https://doi.org/10.1016/j.energy.2020.117116.
[38] G. Xia, H. Zhao, J. Zhang, H. Yang, B. Feng, Q. Zhang, et al., Study on performance of the thermoelectric cooling device with novel subchannel finned heat sink, Energies 15 (1) (2021) 145, https://doi.org/10.3390/en15010145.
[39] J. Christopher, OpenFOAM User Guide Version 10, The OpenFOAM Foundation, Greenshields, 2022.
[40] C.Y. Du, C.D. Wen, Experimental investigation and numerical analysis for one-stage thermoelectric cooler considering Thomson effect, Int. J. Heat Mass Tran. 54 (23–24) (2011) 4875–4884, https://doi.org/10.1016/j.ijheatmasstransfer.2011.06.043.
[41] D. Guo, Q. Sheng, X. Dou, Z. Wang, L. Xie, B. Yang, Application of thermoelectric cooler in temperature control system of space science experiment, Appl. Therm. Eng. 168 (2020), 114888, https://doi.org/10.1016/j.applthermaleng.2019.114888.
[42] Y.K. Kang, H. Lim, S.Y. Cheon, J.W. Jeong, Phase-change material-integrated thermoelectric radiant panel: experimental performance analysis and system design, Appl. Therm. Eng. 194 (2021), 117082, https://doi.org/10.1016/j.applthermaleng.2021.117082.